

---

# Augmented Sliced Wasserstein Distances

---

Xiongjie Chen, Yongxin Yang and Yunpeng Li

University of Surrey

{xiongjie.chen, yongxin.yang, yunpeng.li}@surrey.ac.uk

## Abstract

While theoretically appealing, the application of the Wasserstein distance to large-scale machine learning problems has been hampered by its prohibitive computational cost. The sliced Wasserstein distance and its variants improve the computational efficiency through random projection, yet they suffer from low projection efficiency because the majority of projections result in trivially small values. In this work, we propose a new family of distance metrics, called augmented sliced Wasserstein distances (ASWDs), constructed by first mapping samples to higher-dimensional hypersurfaces parameterized by neural networks. It is derived from a key observation that (random) linear projections of samples residing on these hypersurfaces would translate to much more flexible *nonlinear* projections in the original sample space, so they can capture complex structures of the data distribution. We show that the hypersurfaces can be optimized by gradient ascent efficiently. We provide the condition under which the ASWD is a valid metric and show that this can be obtained by an injective neural network architecture. Numerical results demonstrate that the ASWD significantly outperforms other Wasserstein variants for both synthetic and real-world problems.

## 1 Introduction

Comparing samples from two probability distributions is a fundamental problem in statistics and machine learning. The optimal transport (OT) theory [Villani, 2008] provides a powerful and flexible theoretical tool to compare degenerative distributions by accounting for the metric in the underlying spaces. The Wasserstein distance, which arises from the optimal transport theory, has become an increasingly popular choice in various machine learning domains ranging from generative models to transfer learning [Gulrajani et al., 2017; Arjovsky et al., 2017; Kolouri et al., 2018; Lee et al., 2019; Cuturi and Doucet, 2014; Claici et al., 2018; Courty et al., 2016; Shen et al., 2018; Patrini et al., 2018].

Despite its favorable properties, such as robustness to disjoint supports and numerical stability [Arjovsky et al., 2017], the Wasserstein distance suffers from high computational complexity especially when the sample size is large. Besides, the Wasserstein distance itself is the result of an optimization problem — it is non-trivial to be integrated into an end-to-end training pipeline of deep neural networks, unless one can make the solver for the optimization problem differentiable. Recent advances in computational optimal transport methods focus on alternative OT-based metrics that are computationally efficient and differentiably solvable [Peyré and Cuturi, 2019]. Entropy regularization is introduced in the Sinkhorn distance [Cuturi, 2013] and its variants [Altschuler et al., 2017; Dessein et al., 2018; Lin et al., 2019] to smooth the optimal transport problem; as a result, iterative matrix scaling algorithms can be applied to provide significantly faster solutions with improved sample complexity [Genevay et al., 2019].

An alternative approach is to approximate the Wasserstein distance through *slicing*, i.e. linearly projecting, the distributions to be compared. The sliced Wasserstein distance (SWD) [Bonneel et al., 2015] is defined as the expected value of Wasserstein distances between one-dimensional random projections of high-dimensional distributions. The SWD shares similar theoretical properties with the

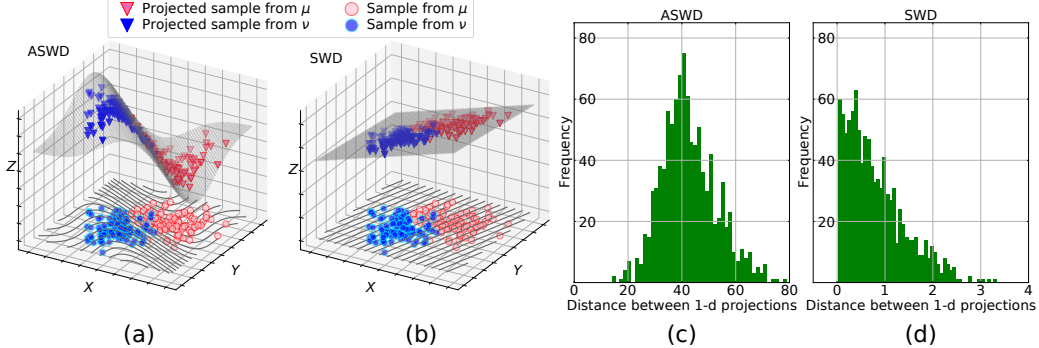


Figure 1: (a) and (b) are visualizations of projections for the ASWD and the SWD between two 2-dimensional Gaussians. (c) and (d) are distance histograms for the ASWD and the SWD between two 100-dimensional Gaussians. Figure 1(a) shows that the injective neural network embedded in the ASWD learns data patterns (in the  $X$ - $Y$  plane) and produces well-separate projected values (Z-axis) between distributions in a random projection direction. The high projection efficiency of the ASWD is evident in Figure 1(c), as almost all random projection directions in a 100-dimensional space lead to significant distances between 1-dimensional projections. In contrast, random linear mappings in the SWD often produce closer 1-d projections (Z-axis) (Figure 1(b)); as a result, a large percentage of random projection directions in the 100-d space result in trivially small distances (Figure 1(d)), leading to a low projection efficiency in high-dimensional spaces.

Wasserstein distance [Bonnotte, 2013] and is computationally efficient since the Wasserstein distance in one-dimensional space has a closed form solution based on sorting. [Deshpande et al., 2019] extends the sliced Wasserstein distance to the max-sliced Wasserstein distance (max-SWD), by finding a single projection direction with the maximal distance between projected samples. In [Nguyen et al., 2020], the distributional sliced Wasserstein distance (DSWD) finds a distribution of projections that maximizes the expected distances over these projections. The subspace robust Wasserstein distance extends the idea of slicing to projecting distributions on linear subspaces [Paty and Cuturi, 2019]. However, the linear nature of these projections usually leads to low projection efficiency of the resulted metrics in high-dimensional spaces [Deshpande et al., 2019; Liutkus et al., 2019; Kolouri et al., 2019].

More recently, there are growing interests and evidences that slice-based Wasserstein distances with nonlinear projections can improve the projection efficiency, leading to a reduced number of projections needed to capture the structure of the data distribution [Kolouri et al., 2019; Nguyen et al., 2020]. [Kolouri et al., 2019] extends the connection between the sliced Wasserstein distance and the Radon transform [Abraham et al., 2017] to define generalized sliced Wasserstein distances (GSWDs) by utilizing generalized Radon transforms (GRTs). It is shown in [Kolouri et al., 2019] that the GSWD is indeed a metric if and only if the adopted GRT is injective. Injective GRTs are also used to extend the DSWD to the distributional generalized sliced Wasserstein distance (DGSWD) [Nguyen et al., 2020]. However, both the GSWD and the DGSWD are restricted by the limited class of injective GRTs, which include the circular Radon transform and a finite number of harmonic polynomial functions with odd degrees [Kuchment, 2006; Ehrenpreis, 2003]. The results reported in [Kolouri et al., 2019; Nguyen et al., 2020] show impressive performance from the GSWD and the DGSWD, yet they require the specification of problem-specific GRTs. One variant of the GSWD generates projections directly with neural network outputs in order to remove some limitations of the polynomial-based GRTs, but the resulted GSWD becomes a *pseudo-metric* since it is highly non-trivial to prove the injectivity of the associated GRT [Kolouri et al., 2019].

In this paper, we present the augmented sliced Wasserstein distance (ASWD), a distance metric constructed by first mapping samples to hypersurfaces in an *augmented* space, which enables flexible nonlinear slicing of data distributions for improved projection efficiency (See Figure 1). Our main contributions include: (i) We exploit the capacity of nonlinear projections employed in the ASWD by constructing injective mapping with arbitrary neural networks; (ii) We prove that the ASWD is a valid distance metric; (iii) We show that the highly flexible hypersurfaces in the augmented space can be optimized efficiently with gradient ascent; (iv) We demonstrate superior performance of the ASWD in numerical experiments for both synthetic and real-world datasets.

The remainder of the paper is organized as follows. Section 2 reviews the necessary background. We present the proposed method and its numerical implementation in Section 3. Numerical experiment results are presented and discussed in Section 4. We conclude the paper in Section 5.

## 2 Background

In this section, we provide a brief review of concepts related to the proposed work, including the Wasserstein distance, (generalized) Radon transform and (generalized) sliced Wasserstein distances.

**Wasserstein distance:** Let  $P_k(\Omega)$  be a set of Borel probability measures with finite  $k$ -th moment on a Polish metric space  $(\Omega, d)$  [Villani, 2008]. Given two probability measures  $\mu, \nu \in P_k(\Omega)$ , whose probability density functions (PDFs) are  $p_\mu$  and  $p_\nu$ , the Wasserstein distance of order  $k \in [1, +\infty)$  between  $\mu$  and  $\nu$  is defined as:

$$W_k(\mu, \nu) = \left( \inf_{\gamma \in \Gamma(\mu, \nu)} \int_{\Omega} d(x, y)^k d\gamma(x, y) \right)^{\frac{1}{k}}, \quad (1)$$

where  $d(\cdot, \cdot)^k$  is the cost function,  $\Gamma(\mu, \nu)$  represents the set of all transportation plans  $\gamma$ , i.e. joint distributions whose marginals are  $p_\mu$  and  $p_\nu$ , respectively. With a slight abuse of notation, we interchangeably use  $W_k(\mu, \nu)$  and  $W_k(p_\mu, p_\nu)$ .

While the Wasserstein distance is generally intractable for high-dimensional distributions, there are several favorable cases where the optimal transport problem can be efficiently solved. In particular, if  $\mu$  and  $\nu$  are continuous one-dimensional measures, the Wasserstein distance between  $\mu$  and  $\nu$  has a closed form solution [Bonneel et al., 2015]:

$$W_k(\mu, \nu) = \left( \int_0^1 d(F_\mu^{-1}(z), F_\nu^{-1}(z))^k dz \right)^{\frac{1}{k}}, \quad (2)$$

where  $F_\mu^{-1}$  and  $F_\nu^{-1}$  are inverse cumulative distribution functions (CDFs) of  $\mu$  and  $\nu$ , respectively.

**Radon transform and generalized Radon transform:** The Radon transform [Radon, 1917] maps a function  $f(\cdot) \in L^1(\mathbb{R}^d)$  to the space of functions defined over spaces of lines in  $\mathbb{R}^d$ . The Radon transform of  $f(\cdot)$  is defined by line integrals of  $f(\cdot)$  along all possible hyperplanes in  $\mathbb{R}^d$ :

$$\mathcal{R}f(t, \theta) = \int_{\mathbb{R}^d} f(x) \delta(t - \langle x, \theta \rangle) dx, \quad (3)$$

where  $t \in \mathbb{R}$  and  $\theta \in \mathbb{S}^{d-1}$  represent the parameters of hyperplanes in  $\mathbb{R}^d$ ,  $\delta(\cdot)$  is the Dirac delta function, and  $\langle \cdot, \cdot \rangle$  refers to the Euclidean inner product.

By replacing the inner product  $\langle x, \theta \rangle$  in Equation (3) with  $\beta(x, \theta)$ , a specific family of functions named as *defining function* in [Kolouri et al., 2019], the generalized Radon transform (GRT) [Beylkin, 1984] is defined as:

$$\mathcal{G}f(t, \theta) = \int_{\mathbb{R}^d} f(x) \delta(t - \beta(x, \theta)) dx, \quad (4)$$

where  $t \in \mathbb{R}$ ,  $\theta \in \Omega_\theta$  while  $\Omega_\theta$  is a compact set of all feasible  $\theta$ , e.g.  $\Omega_\theta = \mathbb{S}^{d-1}$  for  $\beta(x, \theta) = \langle x, \theta \rangle$  [Kolouri et al., 2019].

In practice, we can empirically approximate the Radon transform and the GRT of a probability density function  $p_\mu$  via:

$$\mathcal{R}p_\mu(t, \theta) \approx \frac{1}{N} \sum_{n=1}^N \delta(t - \langle x_n, \theta \rangle), \quad (5)$$

$$\mathcal{G}p_\mu(t, \theta) \approx \frac{1}{N} \sum_{n=1}^N \delta(t - \beta(x_n, \theta)), \quad (6)$$

where  $x_n \sim p_\mu$  and  $N$  is the number of samples. Notably, the Radon transform is a linear bijection [Helgason, 1980], and the GRT is a bijection if the defining function  $\beta$  satisfies certain conditions [Beylkin, 1984].

**Sliced Wasserstein distance and generalized sliced Wasserstein distance:** By applying the Radon transform to  $p_\mu$  and  $p_\nu$  to obtain multiple projections, the sliced Wasserstein distance (SWD) decomposes the high-dimensional Wasserstein distance into multiple one-dimensional Wasserstein distances which can be efficiently evaluated [Bonneel et al., 2015]. The  $k$ -SWD between  $\mu$  and  $\nu$  is defined by:

$$\text{SWD}_k(\mu, \nu) = \left( \int_{\mathbb{S}^{d-1}} W_k^k(\mathcal{R}p_\mu(\cdot, \theta), \mathcal{R}p_\nu(\cdot, \theta)) d\theta \right)^{\frac{1}{k}}, \quad (7)$$

where the Radon transform  $\mathcal{R}$  defined by Equation (3) is adopted as the measure push-forward operator. The GSWD generalizes the idea of SWD by projecting distributions onto hypersurfaces rather than hyperplanes [Kolouri et al., 2019]. The GSWD is defined as:

$$\text{GSWD}_k(\mu, \nu) = \left( \int_{\Omega_\theta} W_k^k(\mathcal{G}p_\mu(\cdot, \theta), \mathcal{G}p_\nu(\cdot, \theta)) d\theta \right)^{\frac{1}{k}}, \quad (8)$$

where the GRT  $\mathcal{G}$  is used as the measure push-forward operator. The Wasserstein distances between one-dimensional distributions can be obtained by sorting projected samples and calculating the distance between sorted samples [Kolouri et al., 2018]: with  $L$  random projections, the SWD and GSWD between  $\mu$  and  $\nu$  can be approximated by:

$$\text{SWD}_k(\mu, \nu) \approx \left( \frac{1}{L} \sum_{l=1}^L \sum_{n=1}^N |\langle x_{I_x^l[n]}, \theta_l \rangle - \langle y_{I_y^l[n]}, \theta_l \rangle|^k \right)^{\frac{1}{k}}, \quad (9)$$

$$\text{GSWD}_k(\mu, \nu) \approx \left( \frac{1}{L} \sum_{l=1}^L \sum_{n=1}^N |\beta(x_{I_x^l[n]}, \theta_l) - \beta(y_{I_y^l[n]}, \theta_l)|^k \right)^{\frac{1}{k}}, \quad (10)$$

where  $I_x^l$  and  $I_y^l$  are sequences consist of the indices of sorted samples which satisfy  $\langle x_{I_x^l[n]}, \theta_l \rangle \leq \langle x_{I_x^l[n+1]}, \theta_l \rangle$ ,  $\langle y_{I_y^l[n]}, \theta_l \rangle \leq \langle y_{I_y^l[n+1]}, \theta_l \rangle$  in the SWD, and  $\beta(x_{I_x^l[n]}, \theta_l) \leq \beta(x_{I_x^l[n+1]}, \theta_l)$ ,  $\beta(y_{I_y^l[n]}, \theta_l) \leq \beta(y_{I_y^l[n+1]}, \theta_l)$  in the GSWD. It is proved in [Bonnotte, 2013] that the SWD is a valid distance metric. The GSWD is a valid metric except for its neural network variant [Kolouri et al., 2019].

### 3 Augmented sliced Wasserstein distances

In this section, we propose a new distance metric called the augmented sliced Wasserstein distance (ASWD), which embeds flexible nonlinear projections in its construction. We also provide an implementation recipe for the ASWD.

#### 3.1 Spatial Radon transform and augmented sliced Wasserstein distance

In the definitions of the SWD and GSWD, the Radon transform [Radon, 1917] and the generalized Radon transform (GRT) [Beylkin, 1984] are used as the push-forward operator for projecting distributions to a one-dimensional space. However, it is not straightforward to design defining functions  $\beta(x, \theta)$  [Kolouri et al., 2019] for the GRT due to certain non-trivial requirements for the function [Beylkin, 1984]. In practice, the assumption of the transform can be relaxed, as Theorem 1 shows that as long as the transform is injective, the corresponding ASWD metric is a valid distance metric.

To help us define the augmented sliced Wasserstein distance, we first introduce a *spatial Radon transform* which includes the vanilla Radon transform and GRTs as special cases (See Remark 2).

**Definition 1.** Given an injective mapping  $g(\cdot) : \mathbb{R}^d \rightarrow \mathbb{R}^{d_\theta}$  and a probability measure  $\mu \in P(\mathbb{R}^d)$  which probability density function (PDF) is  $p_\mu$ , the spatial Radon transform of  $p_\mu$  is defined as

$$\mathcal{H}p_\mu(t, \theta; g) = \int_{\mathbb{R}^d} p_\mu(x) \delta(t - \langle g(x), \theta \rangle) dx, \quad (11)$$

where  $t \in \mathbb{R}$  and  $\theta \in \mathbb{S}^{d_\theta-1}$  are the parameters of hypersurfaces in  $\mathbb{R}^d$ .

**Remark 1.** Note that the spatial Radon transform can be interpreted as applying the vanilla Radon transform to the PDF of  $\hat{x} = g(x)$ , where  $x \sim p_\mu$ . Denote the PDF of  $\hat{x}$  by  $p_{\hat{\mu}_g}$ , the spatial Radon

transform defined by (11) can be rewritten as:

$$\begin{aligned}
\mathcal{H}p_\mu(t, \theta; g) &= E_{x \sim p_\mu} [\delta(t - \langle g(x), \theta \rangle)], \\
&= E_{\hat{x} \sim p_{\hat{\mu}_g}} [\delta(t - \langle \hat{x}, \theta \rangle)] \\
&= \int p_{\hat{\mu}_g}(\hat{x}) \delta(t - \langle \hat{x}, \theta \rangle) d\hat{x} \\
&= \mathcal{R}p_{\hat{\mu}_g}(t, \theta).
\end{aligned} \tag{12}$$

Hence the spatial Radon transform inherits the theoretical properties of the Radon transform subject to certain conditions of  $g(\cdot)$  and incorporates nonlinear projections through  $g(\cdot)$ .

In what follows, we use  $f_1 \equiv f_2$  to denote functions  $f_1(\cdot) : X \rightarrow \mathbb{R}$  and  $f_2(\cdot) : X \rightarrow \mathbb{R}$  that satisfy  $f_1(x) = f_2(x)$  for  $\forall x \in X$ .

**Lemma 1.** *Given an injective mapping  $g(\cdot) : \mathbb{R}^d \rightarrow \mathbb{R}^{d_\theta}$  and two probability measures  $\mu, \nu \in P(\mathbb{R}^d)$  whose probability density functions are  $p_\mu$  and  $p_\nu$ , respectively, for all  $t \in \mathbb{R}$  and  $\theta \in \mathbb{S}^{d_\theta-1}$ ,  $\mathcal{H}p_\mu(t, \theta; g) \equiv \mathcal{H}p_\nu(t, \theta; g)$  if and only if  $p_\mu \equiv p_\nu$ , i.e. the spatial Radon transform is injective. Moreover, the spatial Radon transform is injective if and only if the mapping  $g(\cdot)$  is an injection.*

See Appendix A for the proof of Lemma 1.

**Remark 2.** *The spatial Radon transform degenerates to the vanilla Radon transform when the mapping  $g(\cdot)$  is an identity mapping. When  $g(\cdot)$  is a homogeneous polynomial function with odd degrees, the spatial Radon transform is equivalent to the polynomial GRT [Ehrenpreis, 2003].*

We now introduce the augmented sliced Wasserstein distance, by utilizing the spatial Radon transform as the measure push-forward operator:

**Definition 2.** *Given two probability measures  $\mu, \nu \in P_k(\mathbb{R}^d)$ , whose probability density functions are  $p_\mu$  and  $p_\nu$ , respectively, and an injective mapping  $g(\cdot) : \mathbb{R}^d \rightarrow \mathbb{R}^{d_\theta}$ , the augmented sliced Wasserstein distance (ASWD) of order  $k \in [1, +\infty)$  is defined as:*

$$\text{ASWD}_k(\mu, \nu; g) = \left( \int_{\mathbb{S}^{d_\theta-1}} W_k^k(\mathcal{H}p_\mu(\cdot, \theta; g), \mathcal{H}p_\nu(\cdot, \theta; g)) d\theta \right)^{\frac{1}{k}}, \tag{13}$$

where  $\theta \in \mathbb{S}^{d_\theta-1}$ ,  $W_k$  is the  $k$ -Wasserstein distance defined by Equation (1), and  $\mathcal{H}$  refers to the spatial Radon transform defined by Equation (11).

**Remark 3.** *Following the connection between the spatial Radon transform and the vanilla Radon transform as shown in Equation (12), the ASWD can be rewritten as:*

$$\begin{aligned}
\text{ASWD}_k(\mu, \nu; g) &= \left( \int_{\mathbb{S}^{d_\theta-1}} W_k^k(\mathcal{R}p_{\hat{\mu}_g}(\cdot, \theta), \mathcal{R}p_{\hat{\nu}_g}(\cdot, \theta)) d\theta \right)^{\frac{1}{k}} \\
&= \text{SWD}_k(\hat{\mu}_g, \hat{\nu}_g),
\end{aligned} \tag{14}$$

where  $\hat{\mu}_g$  and  $\hat{\nu}_g$  are probability measures on  $\mathbb{R}^{d_\theta}$  which satisfy  $g(x) \sim \hat{\mu}_g$  for  $x \sim \mu$  and  $g(y) \sim \hat{\nu}_g$  for  $y \sim \nu$ .

**Theorem 1.** *The augmented sliced Wasserstein distance (ASWD) of order  $k \in [1, +\infty)$  defined by Equation (13) with a mapping  $g(\cdot) : \mathbb{R}^d \rightarrow \mathbb{R}^{d_\theta}$  is a metric on  $P_k(\mathbb{R}^d)$  if and only if  $g(\cdot)$  is injective.*

Proof of Theorem 1 is provided in Appendix B.

### 3.2 Numerical implementation

We discuss in this section how to realize injective mapping  $g(\cdot)$  with *neural networks* due to their expressiveness and optimize it with gradient based methods.

**Injective neural networks:** As stated in Lemma 1 and Theorem 1, the injectivity of  $g(\cdot)$  is the sufficient and necessary condition for the ASWD being a valid metric. Thus we need specific architecture designs on implementing  $g(\cdot)$  by neural networks. One option is the family of invertible neural networks [Behrmann et al., 2019; Karami et al., 2019; Song et al., 2019], which are both injective and surjective. However, the running cost of those models is usually much higher than that

of vanilla neural networks. We propose an alternative approach by concatenating the input  $x$  of an arbitrary neural network to its output  $\phi_\omega(x)$ :

$$g_\omega(x) = [x, \phi_\omega(x)]. \quad (15)$$

It is trivial to show that  $g_\omega(x)$  is injective, since different inputs will lead to different outputs. Although embarrassingly simple, this idea of concatenating the input and output of neural networks has found success in preserving information with dense blocks in the DenseNet [Huang et al., 2017], where the input of each layer is injective to the output of all preceding layers.

**Optimization objective:** We aim to project samples to maximally discriminating hypersurfaces between two distributions, so that the projected samples between distributions are most dissimilar subject to certain constraints on the hypersurface, as shown in Figure 1. Similar ideas have been employed to identify important projection directions [Deshpande et al., 2019; Kolouri et al., 2019; Paty and Cuturi, 2019] or a discriminative ground metric [Salimans et al., 2018] in optimal transport metrics. For the ASWD, the parameterized injective neural network  $g_\omega(\cdot)$  is optimized by maximizing the following objective:

$$\mathcal{L}(\mu, \nu; g_\omega, \lambda) = \left( \int_{\mathbb{S}^{d_\theta-1}} W_k^k(\mathcal{H}p_\mu(\cdot, \theta; g_\omega), \mathcal{H}p_\nu(\cdot, \theta; g_\omega)) d\theta \right)^{\frac{1}{k}} - L_\lambda, \quad (16)$$

where  $\lambda > 0$  and the regularization term  $L_\lambda = \lambda \mathbb{E}_{x, y \sim \mu, \nu} [(||g_\omega(x)||_2 + ||g_\omega(y)||_2)]$  is used to control the norm of the output of  $g_\omega(\cdot)$ , otherwise the projections may be arbitrarily large.

**Remark 4.** The regularization coefficient  $\lambda$  adjusts the introduced non-linearity in the evaluation of the ASWD by controlling the norm of  $\phi_\omega(\cdot)$  in Equation (15). In particular, when  $\lambda \rightarrow \infty$ , the nonlinear term  $\phi_\omega(\cdot)$  shrinks to 0. The rank of the augmented space is hence explicitly controlled by the flexible choice of  $\phi_\omega(\cdot)$  and implicitly regularized by  $L_\lambda$ .

By plugging the optimized  $g_{\omega, \lambda}^*(\cdot) = \operatorname{argmax}_{g_\omega}(\mathcal{L}(\mu, \nu; g_\omega, \lambda))$  into Equation (13), we obtain the empirical version of the ASWD. Pseudocode is provided in Appendix C.

## 4 Experiments

In this section, we describe the experiments that we have conducted to evaluate performance of the proposed distance metric. The GSWD leads to the best performance in a sliced Wasserstein flow problem reported in [Kolouri et al., 2019] and the DSWD outperforms the compared methods in the generating modeling task examined in [Nguyen et al., 2020]. Hence we compare performance of the ASWD with the state-of-the-art distance metrics in the same examples and report results as below<sup>1</sup>.

To examine the robustness of the ASWD, throughout the experiments, we adopt the injective network architecture given in Equation (15) and set  $\phi_\omega$  to be a one layer fully-connected neural network whose outputs' dimension equals its inputs' dimension.

### 4.1 Sliced Wasserstein flows

We first consider the problem of evolving a source distribution  $\mu$  to a target distribution  $\nu$  by minimizing Wasserstein distances between  $\mu$  and  $\nu$  in the sliced Wasserstein flow task reported in [Kolouri et al., 2019].

$$\partial_t \mu_t = -\nabla \text{SWD}(\mu_t, \nu), \quad (17)$$

where  $\mu_t$  refers to the updated source distribution at each iteration  $t$ . The SWD in Equation (17) can be replaced by other sliced-Wasserstein distances to be evaluated. As in [Kolouri et al., 2019], the 2-Wasserstein distance was used as the metric for evaluating performance of different distance metrics in this task. The set of hyperparameter values used in this experiment can be found in Appendix D.1.

Without loss of generality, we initialize  $\mu_0$  to be the standard normal distribution  $\mathcal{N}(0, I)$ . We repeat each experiment 50 times and record the 2-Wasserstein distance between  $\mu$  and  $\nu$  at every iteration. In Figure 2, we plot the 2-Wasserstein distances between the source and target distributions as a function

<sup>1</sup>Code to reproduce experiment results is available at this anonymous repository: <https://bit.ly/2Y23w0z>.

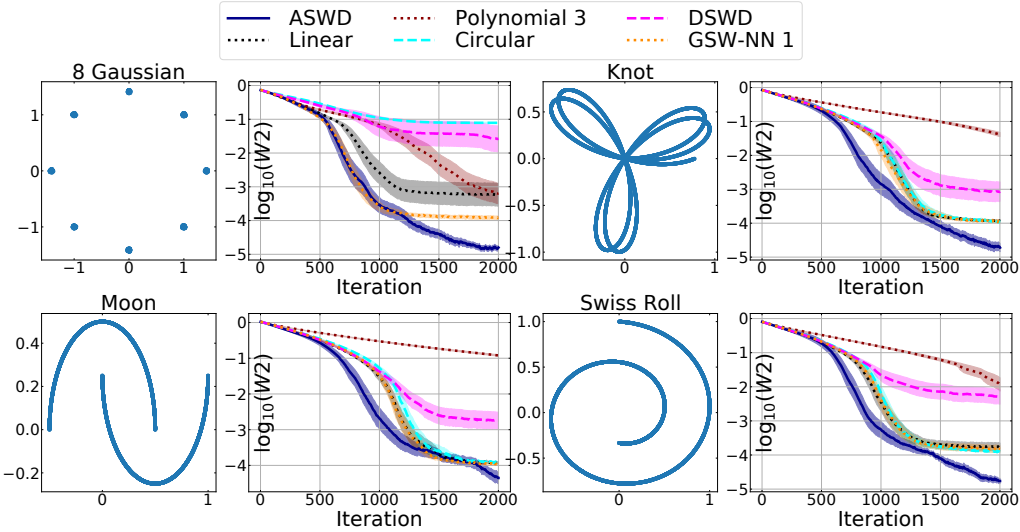


Figure 2: The first and third columns are target distributions. The second and fourth columns are  $\log 2$ -Wasserstein distances between the target distribution and the source distribution. The horizontal axis show the number of training iterations. Solid lines and shaded areas represent the average values and 95% confidence intervals of  $\log 2$ -Wasserstein distances over 50 runs. A more extensive set of experimental results can be found in Appendix E.

of the training epochs and the 8-Gaussian, the Knot, the Moon, and the Swiss roll distributions are respective target distributions. For clarity, Figure 2 displays the experiment results from the 6 best performing distance metrics, including the ASWD, the DSWD, the SWD as well as the GSWD with the circular, polynomial with degree 3 and one layer MLP defining functions, out of the 12 distance metrics we compared.

We observe from Figure 2 that the ASWD not only leads to lower 2-Wasserstein distances, but also converges faster by achieving better results with fewer iterations than the other methods in these four target distributions. A complete set of experimental results with 12 compared distance metrics and 8 target distributions are included in Appendix E. The ASWD outperforms the compared state-of-the-art sliced-based Wasserstein distance metrics with 7 out of the 8 target distributions except for the 25-Gaussian. This is achieved through the simple injective network architecture given in Equation (15) and a one layer fully-connected neural network with equal input and output dimensions throughout the experiments. Future directions include further improving its robustness over more distributions and investigating the impact of other types of network architecture, e.g. invertible neural networks, as candidate injective mapping functions.

## 4.2 Generative modeling

In this experiment, we use the sliced-based Wasserstein distances for a generative modeling task described in [Nguyen et al., 2020]. The task is to generate images using generative adversarial networks (GANs) [Goodfellow et al., 2014] trained on either the CIFAR10 dataset ( $64 \times 64$  resolution) [Krizhevsky, 2009] or the CELEBA dataset ( $64 \times 64$  resolution) [Liu et al., 2015]. Denote the hidden layer and the output layer of the discriminator by  $h_\psi$  and  $D_\Psi$ , and the generator by  $G_\Phi$ , we train GAN models with the following objectives:

$$\min_{\Phi} \text{SWD}(h_\psi(p_r), h_\psi(G_\Phi(p_z))), \quad (18)$$

$$\max_{\Psi, \psi} \mathbb{E}_{x \sim p_r} [\log(D_\Psi(h_\psi(x)))] + \mathbb{E}_{z \sim p_z} [\log(1 - D_\Psi(h_\psi(G_\Phi(z)))] \quad (19)$$

where  $p_z$  is the prior of latent variable  $z$  and  $p_r$  is the distribution of real data. The SWD in Equation (18) is replaced by the ASWD and other variants of the SWD to compare their performance. The GSWD with the polynomial defining function and the DGSWD is not included in this experiment due to its excessively high computational cost in high-dimensional space. The *Fréchet Inception Distance*

Table 1: FID scores of generative models trained with different distance metrics. Lower scores indicate better image qualities.  $L$  is the number of projections, we run each experiment 10 times and report the average values and standard errors of FID scores for CIFAR10 dataset and CELEBA dataset. The running time per training iteration for one batch containing 512 samples is computed based on a computer with an Intel (R) Xeon (R) Gold 5218 CPU 2.3 GHz and 16GB of RAM, and a RTX 6000 graphic card with 22GB memories.

CIFAR10									
$L$	SWD		GSWD		DSWD		ASWD		
	FID	$t$ (s/it)	FID	$t$ (s/it)	FID	$t$ (s/it)	FID	$t$ (s/it)	
10	192.6 $\pm$ 5.7	0.32	189.5 $\pm$ 6.0	0.35	79.0 $\pm$ 4.2	0.48	<b>73.2<math>\pm</math>3.1</b>	0.55	
100	155.0 $\pm$ 2.9	0.32	155.9 $\pm$ 3.2	0.70	72.2 $\pm$ 8.2	0.51	<b>66.7<math>\pm</math>3.2</b>	0.57	
1000	126.0 $\pm$ 2.9	0.34	134.5 $\pm$ 2.7	2.10	74.3 $\pm$ 4.3	1.22	<b>65.5<math>\pm</math>3.9</b>	1.32	
CELEBA									
10	118.3 $\pm$ 3.1	0.32	143.2 $\pm$ 5.5	0.35	105.3 $\pm$ 3.4	0.49	<b>99.2<math>\pm</math>4.3</b>	0.53	
100	116.0 $\pm$ 2.8	0.33	120.8 $\pm$ 1.8	0.69	103.1 $\pm$ 3.8	0.51	<b>94.3<math>\pm</math>2.2</b>	0.56	
1000	104.4 $\pm$ 2.8	0.34	101.8 $\pm$ 1.8	2.14	97.4 $\pm$ 2.1	1.21	<b>90.5<math>\pm</math>3.0</b>	1.31	

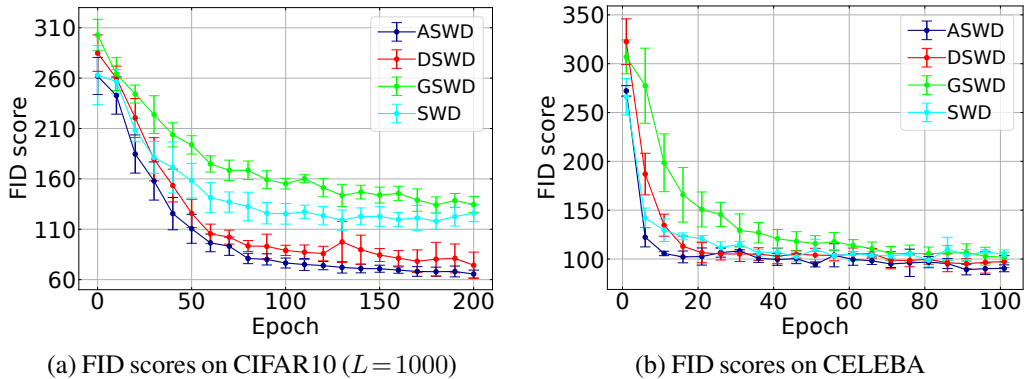


Figure 3: FID scores of generative models trained with different metrics on CIFAR10 and CELEBA datasets with  $L = 1000$  projections. The error bar represents the standard deviation of the FID scores at the specified training epoch among 10 simulation runs.

(FID score) [Heusel et al., 2017] is used to assess the quality of generated images. More details on the network structures and the parameter setup used in this experiment are available in Appendix D.2.

We run 200 and 100 training epochs to train the GAN models on the CIFAR10 and the CELEBA dataset, respectively. Each experiment is repeated for 10 times. We report experimental results in Table 1. With the same number of projections and a similar computation cost, the ASWD leads to significantly improved FID scores among all evaluated distances metrics on both datasets, which implies that images generated with the ASWD are of higher qualities. Figure 3 plots the FID scores recorded during the training process. The GAN model trained with the ASWD exhibits a faster convergence as it reaches lower FID scores with fewer epochs. Randomly selected samples of generated images are presented in Appendix F.

## 5 Conclusion

We proposed a novel variant of the sliced Wasserstein distance, namely the augmented sliced Wasserstein distance (ASWD), which is flexible, has high sample efficiency, and generalizes well. The ASWD adaptively updates the hypersurface where the samples are projected onto by learning from data. We proved that the ASWD is a valid distance metric and presented its numerical implementation. We reported empirical performance of the ASWD over state-of-the-art sliced Wasserstein metrics in numerical experiments. The ASWD leads to the smallest distance errors over the majority of datasets in a sliced Wasserstein flow task and superior performance in a generative modeling task.

## Broader impact

Research on comparing samples drawn from two probability distributions is inherently theoretical; it is also a fundamental topic in statistics and machine learning with a broad spectrum of downstream applications. In particular, our work has its root in the optimal transport theory and can be incorporated in a wide range of applications including computer vision (image retrieval and generation), natural language processing (alignment of word embedding for machine translation) and economics (resource allocation). Hence, this work developed a foundational tool with long-term societal and economic impact; the exact impact will be determined by the particular downstream applications. For example, the proposed distance metric can be used in machine translation to foster greater cross-cultural communication or employed in generative models to create new images or sound as a creativity tool; but it may also be used to produce ‘fake’ images for potentially harmful purposes. Those specific applications and their risk mitigation strategies are active research areas and out of the scope of this work, since this paper focuses on the theoretical and algorithmic development of a computational statistics tool.

## References

I. Abraham, R. Abraham, M. Bergounioux, and G. Carlier. Tomographic reconstruction from a few views: a multi-marginal optimal transport approach. *Applied Mathematics & Optimization*, 75(1):55–73, 2017.

J. Altschuler, J. Niles-Weed, and P. Rigollet. Near-linear time approximation algorithms for optimal transport via Sinkhorn iteration. In *Proc. Advances in Neural Information Processing Systems (NeurIPS)*, pages 1964–1974, Long Beach, California, USA, 2017.

M. Arjovsky, S. Chintala, and L. Bottou. Wasserstein generative adversarial networks. In *Proc. International Conference on Machine Learning (ICML)*, pages 214–223, Sydney, Australia, 2017.

J. Behrmann, W. Grathwohl, R. T. Q. Chen, D. Duvenaud, and J. Jacobsen. Invertible residual networks. In *Proc. International Conference on Machine Learning (ICML)*, pages 573–582, Long Beach, California, USA, 2019.

G. Beylkin. The inversion problem and applications of the generalized Radon transform. *Communications on Pure and Applied Mathematics*, 37(5):579–599, 1984.

N. Bonneel, J. Rabin, G. Peyré, and H. Pfister. Sliced and Radon Wasserstein barycenters of measures. *Journal of Mathematical Imaging and Vision*, 51(1):22–45, 2015.

N. Bonnotte. *Unidimensional and evolution methods for optimal transportation*. PhD thesis, Paris 11, 2013.

S. Claić, E. Chien, and J. Solomon. Stochastic Wasserstein barycenters. In *Proc. International Conference on Machine Learning (ICML)*, pages 999–1008, Stockholm, Sweden, 2018.

N. Courty, R. Flamary, D. Tuia, and A. Rakotomamonjy. Optimal transport for domain adaptation. *IEEE Transactions on Pattern Analysis and Machine Intelligence (IPAMI)*, 39(9):1853–1865, 2016.

M. Cuturi. Sinkhorn distances: Lightspeed computation of optimal transport. In *Proc. Advances in Neural Information Processing Systems (NeurIPS)*, pages 2292–2300, Lake Tahoe, Nevada, USA, 2013.

M. Cuturi and A. Doucet. Fast computation of Wasserstein barycenters. In *Proc. International Conference on Machine Learning (ICML)*, pages 685–693, Beijing, China, 2014.

I. Deshpande et al. Max-sliced Wasserstein distance and its use for GANs. In *Proc. IEEE Conference on Computer Vision and Pattern Recognition (CVPR)*, pages 10648–10656, Long Beach, California, USA, 2019.

A. Dessein, N. Papadakis, and J. Rouas. Regularized optimal transport and the rot mover’s distance. *The Journal of Machine Learning Research (JMLR)*, 19(1):590–642, 2018.

L. Ehrenpreis. *The universality of the Radon transform*, chapter 5, pages 299–363. Oxford University Press, Oxford, UK, 2003.

A. Genevay, L. Chizat, F. Bach, M. Cuturi, and G. Peyré. Sample complexity of Sinkhorn divergences. In *International Conference on Artificial Intelligence and Statistics (AISTATS)*, pages 1574–1583, Okinawa, Japan, 2019.

I. Goodfellow et al. Generative adversarial nets. In *Proc. Advances in Neural Information Processing Systems (NeurIPS)*, pages 2672–2680, Montréal, Canada, 2014.

I. Gulrajani, F. Ahmed, M. Arjovsky, V. Dumoulin, and A. Courville. Improved training of Wasserstein GANs. In *Proc. Advances in neural information processing systems (NeurIPS)*, pages 5767–5777, Long Beach, California, USA, 2017.

S. Helgason. *The Radon transform*, volume 2. Basel, Switzerland: Springer, 1980.

M. Heusel, H. Ramsauer, T. Unterthiner, B. Nessler, and S. Hochreiter. GANs trained by a two time-scale update rule converge to a local Nash equilibrium. In *Proc. Advances in neural information processing systems (NeurIPS)*, pages 6626–6637, Long Beach, California, USA, 2017.

G. Huang, Z. Liu, L. Van Der Maaten, and K. Q. Weinberger. Densely connected convolutional networks. In *Proc. IEEE Conference on Computer Vision and Pattern Recognition (CVPR)*, pages 4700–4708, Hawaii, USA, 2017.

M. Karami, D. Schuurmans, J. Sohl-Dickstein, L. Dinh, and D. Duckworth. Invertible convolutional flow. In *Proc. Advances in Neural Information Processing Systems (NeurIPS)*, pages 5636–5646, Vancouver, Canada, 2019.

D. P. Kingma and J. Ba. Adam: A method for stochastic optimization. In *Proc. International Conference on Learning Representations (ICLR)*, San Diego, California, USA, 2015.

S. Kolouri, P. E. Pope, C. E. Martin, and G. K. Rohde. Sliced-Wasserstein autoencoder: An embarrassingly simple generative model. *arXiv:1804.01947*, 2018.

S. Kolouri, K. Nadjahi, U. Simsekli, R. Badeau, and G. Rohde. Generalized sliced Wasserstein distances. In *Proc. Advances in Neural Information Processing Systems (NeurIPS)*, pages 261–272, Vancouver, Canada, 2019.

A. Krizhevsky. Learning multiple layers of features from tiny images. *Tech Report*, 2009.

P. Kuchment. Generalized transforms of Radon type and their applications. In *Proc. Symposia in Applied Mathematics*, volume 63, page 67, San Antonio, Texas, USA, 2006.

C. Lee, T. Batra, M. B. Baig, and D. Ulbricht. Sliced Wasserstein discrepancy for unsupervised domain adaptation. In *Proc. IEEE Conference on Computer Vision and Pattern Recognition (CVPR)*, pages 10285–10295, Long Beach, California, USA, 2019.

T. Lin, N. Ho, and M. I. Jordan. On efficient optimal transport: an analysis of greedy and accelerated mirror descent algorithms. *University of California, Berkeley*, 2019.

Z. Liu, P. Luo, X. Wang, and X. Tang. Deep learning face attributes in the wild. In *Proc. IEEE International Conference on Computer Vision (ICCV)*, pages 3730–3738, Las Condes, Chile, 2015.

A. Liutkus, U. Simsekli, S. Majewski, Szymon, A. D., and F. Stöter. Sliced-Wasserstein flows: Nonparametric generative modeling via optimal transport and diffusions. In *Proc. International Conference on Machine Learning (ICML)*, pages 4104–4113, 2019.

K. Nguyen, N. Ho, T. Pham, and H. Bui. Distributional sliced-Wasserstein and applications to generative modeling. *arXiv:2002.07367*, 2020.

G. Patrini et al. Sinkhorn autoencoders. *arXiv:1810.01118*, 2018.

F. Paty and M. Cuturi. Subspace robust Wasserstein distances. In *Proc. International Conference on Machine Learning (ICML)*, pages 5072–5081, Long Beach, California, USA, 2019.

G. Peyré and M. Cuturi. Computational optimal transport. *Foundations and Trends® in Machine Learning*, 11(5-6):355–607, 2019.

J. Radon. Über die bestimmung von funktionen durch ihre integralwerte laengs gewisser mannigfaltigkeiten. *Ber. Verh. Saechs. Akad. Wiss. Leipzig Math. Phys. Kl.*, 69:262, 1917.

T. Salimans, H. Zhang, A. Radford, and D. Metaxas. Improving GANs using optimal transport. In *Proc. International Conference on Learning Representations (ICLR)*, Vancouver, Canada, 2018.

J. Shen, Y. Qu, W. Zhang, and Y. Yu. Wasserstein distance guided representation learning for domain adaptation. In *Proc. AAAI Conference on Artificial Intelligence (AAAI)*, pages 4058–4065, New Orleans, Louisiana, USA, 2018.

Y. Song, C. Meng, and S. Ermon. Mintnet: Building invertible neural networks with masked convolutions. In *Proc. Advances in Neural Information Processing Systems*, pages 11002–11012, Vancouver, Canada, 2019.

C. Villani. *Optimal Transport: old and new*, volume 338. Berlin, Germany: Springer Science & Business Media, 2008.

## Appendix A Proof of the injectivity of the spatial Radon transform

We prove that the spatial Radon transform defined with a mapping  $g(\cdot) : \mathbb{R}^d \rightarrow \mathbb{R}^{d_\theta}$  is injective if and only if  $g(\cdot)$  is injective. In the following contents, we use  $P_k(\mathbb{R}^d)$  to denote a set of Borel probability measures with finite  $k$ -th moment on  $\mathbb{R}^d$ , and  $f_1 \equiv f_2$  is used to denote functions  $f_1(\cdot) : X \rightarrow \mathbb{R}$  and  $f_2(\cdot) : X \rightarrow \mathbb{R}$  that satisfy  $f_1(x) = f_2(x)$  for  $\forall x \in X$ , and  $f_1 \not\equiv f_2$  is used to denote functions  $f_1(\cdot) : X \rightarrow \mathbb{R}$  and  $f_2(\cdot) : X \rightarrow \mathbb{R}$  that satisfy  $f_1(x) \neq f_2(x)$  for certain  $x \in X$ . With a slight abuse of notation, we interchangeably use  $f_1(x) \equiv f_2(x)$  for  $\forall x \in X$  and  $f_1 \equiv f_2$ .

*Proof.* By using proof by contradiction, we first prove that if  $g(\cdot)$  is injective, the corresponding spatial Radon transform is injective. If the spatial Radon transform defined with an injective mapping  $g(\cdot) : \mathbb{R}^d \rightarrow \mathbb{R}^{d_\theta}$  is not injective, there exist  $\mu, \nu \in P_k(\mathbb{R}^d)$ ,  $\mu \not\equiv \nu$ , such that  $\mathcal{H}p_\mu(t, \theta; g) \equiv \mathcal{H}p_\nu(t, \theta; g)$  for  $\forall t \in \mathbb{R}$  and  $\forall \theta \in \mathbb{S}^{d_\theta-1}$ , where  $p_\mu$  and  $p_\nu$  are probability density functions defined on  $\mathbb{R}^d$  and  $p_\mu \not\equiv p_\nu$ .

From Equation (12), for  $\forall t \in \mathbb{R}$  and  $\forall \theta \in \mathbb{S}^{d_\theta-1}$ , the spatial Radon transform can be written as:

$$\mathcal{H}p_\mu(t, \theta; g) = \mathcal{R}p_{\hat{\mu}_g}(t, \theta), \quad (20)$$

$$\mathcal{H}p_\nu(t, \theta; g) = \mathcal{R}p_{\hat{\nu}_g}(t, \theta), \quad (21)$$

where  $p_{\hat{\mu}_g}$  and  $p_{\hat{\nu}_g}$  refer to the probability density functions of  $\hat{x} = g(x)$  and  $\hat{y} = g(y)$  respectively, where  $x \sim \mu$  and  $y \sim \nu$ . From Equations (20) and (21), we know  $\mathcal{R}p_{\hat{\mu}_g}(t, \theta) \equiv \mathcal{R}p_{\hat{\nu}_g}(t, \theta)$  for  $\forall t \in \mathbb{R}$  and  $\forall \theta \in \mathbb{S}^{d_\theta-1}$ , which implies  $p_{\hat{\mu}_g} \equiv p_{\hat{\nu}_g}$  as the Radon transform is injective.

Since  $g(\cdot)$  is injective, for  $\forall \mathcal{X} \subseteq \mathbb{R}^d$ ,  $x \in \mathcal{X}$  if and only if  $\hat{x} = g(x) \in g(\mathcal{X})$ , which implies  $P(x \in \mathcal{X}) = P(\hat{x} \in g(\mathcal{X}))$ ,  $P(y \in \mathcal{X}) = P(\hat{y} \in g(\mathcal{X}))$ . Therefore,

$$\int_{g(\mathcal{X})} p_{\hat{\mu}_g}(\hat{x}) d\hat{x} = \int_{\mathcal{X}} p_\mu(x) dx, \quad (22)$$

$$\int_{g(\mathcal{X})} p_{\hat{\nu}_g}(\hat{y}) d\hat{y} = \int_{\mathcal{X}} p_\nu(y) dy. \quad (23)$$

Since  $p_{\hat{\mu}_g} \equiv p_{\hat{\nu}_g}$ , from Equations (22) and (23):  $\int_{\mathcal{X}} p_\mu(x) dx = \int_{\mathcal{X}} p_\nu(y) dy$  for  $\forall \mathcal{X} \subseteq \mathbb{R}^d$ . Hence, for  $\forall \mathcal{X} \subseteq \mathbb{R}^d$ :

$$\int_{\mathcal{X}} (p_\mu(x) - p_\nu(x)) dx = 0, \quad (24)$$

which implies  $p_\mu \equiv p_\nu$ , contradicting with the assumption  $p_\mu \not\equiv p_\nu$ . Therefore, if  $\mathcal{H}p_\mu \equiv \mathcal{H}p_\nu$ ,  $p_\mu \equiv p_\nu$ . In addition, from the definition of the spatial Radon transform in Equation (11), it is trivial to show that if  $p_\mu \equiv p_\nu$ ,  $\mathcal{H}p_\mu(t, \theta; g) \equiv \mathcal{H}p_\nu(t, \theta; g)$ . Therefore,  $\mathcal{H}p_\mu \equiv \mathcal{H}p_\nu$  if and only if  $p_\mu \equiv p_\nu$ , i.e. the spatial Radon transform  $\mathcal{H}$  defined with an injective mapping  $g(\cdot) : \mathbb{R}^d \rightarrow \mathbb{R}^{d_\theta}$  is injective.

We now prove that if the spatial Radon transform defined with a mapping  $g(\cdot) : \mathbb{R}^d \rightarrow \mathbb{R}^{d_\theta}$  is injective,  $g(\cdot)$  must be injective. Again, we use proof by contradiction. If  $g(\cdot)$  is not injective, there exist  $x_0, y_0 \in \mathbb{R}^d$  such that  $x_0 \neq y_0$  and  $g(x_0) = g(y_0)$ . For two Dirac measures  $\mu_1$  and  $\nu_1$  which probability density functions are  $p_{\mu_1}(x) = \delta(x - x_0)$  and  $p_{\nu_1}(y) = \delta(y - y_0)$ , respectively, we know  $\mu_1 \not\equiv \nu_1$  as  $x_0 \neq y_0$ .

We define variables  $x \sim \mu_1$  and  $y \sim \nu_1$ . Then for variables  $\hat{x} = g(x)$  and  $\hat{y} = g(y)$ , we denote their probability density functions by  $p_{\mu_2}$  and  $p_{\nu_2}$ , respectively. It is trivial to derive

$$p_{\mu_2}(\hat{x}) = \delta(\hat{x} - g(x_0)), \quad (25)$$

$$p_{\nu_2}(\hat{y}) = \delta(\hat{y} - g(y_0)), \quad (26)$$

which implies  $p_{\mu_2} \equiv p_{\nu_2}$  as  $g(x_0) = g(y_0)$ .

From Equations (20), (21), (25) and (26), for  $\forall t \in \mathbb{R}$  and  $\forall \theta \in \mathbb{S}^{d_\theta-1}$ :

$$\begin{aligned} \mathcal{H}p_{\mu_1}(t, \theta; g) &= \mathcal{R}p_{\mu_2}(t, \theta), \\ &= \mathcal{R}p_{\nu_2}(t, \theta), \\ &= \mathcal{H}p_{\nu_1}(t, \theta; g), \end{aligned} \quad (27)$$

which implies  $\mathcal{H}p_{\mu_1} \equiv \mathcal{H}p_{\nu_1}$ , contradicting with the assumption that the spatial Radon transform is injective. Therefore, if the spatial Radon transform is injective,  $g(\cdot)$  must be injective. We conclude that the spatial Radon transform is injective if and only if the mapping  $g(\cdot)$  is an injection.  $\square$

## Appendix B Proof of Theorem 1

We provide a proof that the ASWD defined with a mapping  $g(\cdot) : \mathbb{R}^d \rightarrow \mathbb{R}^{d_\theta}$  is a metric on  $P_k(\mathbb{R}^d)$ , if and only if  $g(\cdot)$  is injective. In what follows, we denote a set of Borel probability measures with finite  $k$ -th moment on  $\mathbb{R}^d$  by  $P_k(\mathbb{R}^d)$ , and use  $\mu, \nu \in P_k(\mathbb{R}^d)$  to refer to two probability measures whose probability density functions are  $p_\mu$  and  $p_\nu$ .

**Proof. Symmetry:** Since the  $k$ -Wasserstein distance is a metric thus symmetric [Villani, 2008]:

$$W_k(\mathcal{H}p_\mu(\cdot, \theta; g), \mathcal{H}p_\nu(\cdot, \theta; g)) = W_k(\mathcal{H}p_\nu(\cdot, \theta; g), \mathcal{H}p_\mu(\cdot, \theta; g)). \quad (28)$$

Therefore,

$$\begin{aligned} \text{ASWD}_k(\mu, \nu; g) &= \left( \int_{\mathbb{S}^{d_\theta-1}} W_k^k(\mathcal{H}p_\mu(\cdot, \theta; g), \mathcal{H}p_\nu(\cdot, \theta; g)) d\theta \right)^{\frac{1}{k}} \\ &= \left( \int_{\mathbb{S}^{d_\theta-1}} W_k^k(\mathcal{H}p_\nu(\cdot, \theta; g), \mathcal{H}p_\mu(\cdot, \theta; g)) d\theta \right)^{\frac{1}{k}} \\ &= \text{ASWD}_k(\nu, \mu; g). \end{aligned} \quad (29)$$

**Triangle inequality:** Given an injective mapping  $g(\cdot) : \mathbb{R}^d \rightarrow \mathbb{R}^{d_\theta}$  and probability measures  $\mu_1, \mu_2, \mu_3 \in P_k(\mathbb{R}^d)$ , since the  $k$ -Wasserstein distance satisfies the triangle inequality [Villani, 2008], the following inequality holds:

$$\begin{aligned} \text{ASWD}_k(\mu_1, \mu_3; g) &= \left( \int_{\mathbb{S}^{d_\theta-1}} W_k^k(\mathcal{H}p_{\mu_1}(\cdot, \theta; g), \mathcal{H}p_{\mu_3}(\cdot, \theta; g)) d\theta \right)^{\frac{1}{k}} \\ &\leq \left( \int_{\mathbb{S}^{d_\theta-1}} (W_k^k(\mathcal{H}p_{\mu_1}(\cdot, \theta; g), \mathcal{H}p_{\mu_2}(\cdot, \theta; g)) + W_k^k(\mathcal{H}p_{\mu_2}(\cdot, \theta; g), \mathcal{H}p_{\mu_3}(\cdot, \theta; g))) d\theta \right)^{\frac{1}{k}} \\ &\leq \left( \int_{\mathbb{S}^{d_\theta-1}} W_k^k(\mathcal{H}p_{\mu_1}(\cdot, \theta; g), \mathcal{H}p_{\mu_2}(\cdot, \theta; g)) d\theta \right)^{\frac{1}{k}} + \left( \int_{\mathbb{S}^{d_\theta-1}} W_k^k(\mathcal{H}p_{\mu_2}(\cdot, \theta; g), \mathcal{H}p_{\mu_3}(\cdot, \theta; g)) d\theta \right)^{\frac{1}{k}} \\ &= \text{ASWD}_k(\mu_1, \mu_2; g) + \text{ASWD}_k(\mu_2, \mu_3; g), \end{aligned}$$

where the second inequality is due to the Minkowski inequality in  $L^k(\mathbb{S}^{d_\theta-1})$ .

**Identity of indiscernibles:** Since  $W_k(\mu, \mu) = 0$  for  $\forall \mu \in P_k(\mathbb{R}^d)$ , we have

$$\text{ASWD}_k(\mu, \mu; g) = \left( \int_{\mathbb{S}^{d_\theta-1}} W_k^k(\mathcal{H}p_\mu(\cdot, \theta; g), \mathcal{H}p_\mu(\cdot, \theta; g)) d\theta \right)^{\frac{1}{k}} = 0, \quad (30)$$

for  $\forall \mu \in P_k(\mathbb{R}^d)$ .

Conversely, for  $\forall \mu, \nu \in P_k(\mathbb{R}^d)$ , if  $\text{ASWD}_k(\mu, \nu; g) = 0$ , from the definition of the ASWD:

$$\text{ASWD}_k(\mu, \nu; g) = \left( \int_{\mathbb{S}^{d_\theta-1}} W_k^k(\mathcal{H}p_\mu(\cdot, \theta; g), \mathcal{H}p_\nu(\cdot, \theta; g)) d\theta \right)^{\frac{1}{k}} = 0, \quad (31)$$

which implies  $W_k(\mathcal{H}p_\mu(\cdot, \theta; g), \mathcal{H}p_\nu(\cdot, \theta; g)) = 0$  for  $\forall \theta \in \mathbb{S}^{d_\theta-1}$ . Due to the non-negativity of  $k$ -th Wasserstein distance as it is a metric on  $P_k(\mathbb{R}^d)$ ,  $W_k(\mathcal{H}p_\mu(\cdot, \theta; g), \mathcal{H}p_\nu(\cdot, \theta; g)) = 0$  holds for  $\forall \theta \in \mathbb{S}^{d_\theta-1}$  if and only if  $\mathcal{H}p_\mu(\cdot, \theta; g) \equiv \mathcal{H}p_\nu(\cdot, \theta; g)$ . Again, given the spatial Radon transform is injective when  $g(\cdot)$  is injective (see the proof in Appendix A),  $\mathcal{H}p_\mu(\cdot, \theta; g) \equiv \mathcal{H}p_\nu(\cdot, \theta; g)$  implies  $p_\mu \equiv p_\nu$  and  $\mu \equiv \nu$  if  $g(\cdot)$  is injective.

In addition, if  $g(\cdot)$  is not injective, the spatial Radon transform is not injective (see the proof in Appendix A), then  $\exists \mu, \nu \in P_k(\mathbb{R}^d)$ ,  $\mu \neq \nu$  such that  $\mathcal{H}p_\mu(\cdot, \theta; g) \equiv \mathcal{H}p_\nu(\cdot, \theta; g)$ , which implies  $\text{ASWD}_k(\mu, \nu; g) = 0$  for  $\mu \neq \nu$ . Therefore, the ASWD satisfies the identity of indiscernibles if and only if  $g(\cdot)$  is injective.

**Non-negativity:** The three axioms of a distance metric, i.e. symmetry, triangle inequality, and identity of indiscernibles imply the non-negativity of the ASWD. Since the Wasserstein distance is non-negative, for  $\forall \mu, \nu \in P_k(\mathbb{R}^d)$ , it can also be straightforwardly proved the ASWD between  $\mu$  and  $\nu$  is non-negative:

$$\begin{aligned} \text{ASWD}_k(\mu, \nu; g) &= \left( \int_{\mathbb{S}^{d_\theta-1}} W_k^k(\mathcal{H}p_\mu(\cdot, \theta; g), \mathcal{H}p_\nu(\cdot, \theta; g)) d\theta \right)^{\frac{1}{k}} \\ &\geq \left( \int_{\mathbb{S}^{d_\theta-1}} 0^k d\theta \right)^{\frac{1}{k}} = 0. \end{aligned} \quad (32)$$

Therefore, the ASWD is a metric on  $P_k(\mathbb{R}^d)$  if and only if  $g(\cdot)$  is injective.  $\square$

## Appendix C Pseudocode for the empirical version of the ASWD

---

**Algorithm 1** The augmented sliced Wasserstein distance. All of the for loops can be parallelized.

---

**Require:** Sets of samples  $\{x_n \in \mathbb{R}^d\}_{n=1}^N, \{y_n \in \mathbb{R}^d\}_{n=1}^N$ ;  
**Require:** Randomly initialized injective neural network  $g_\omega(\cdot) : \mathbb{R}^d \rightarrow \mathbb{R}^{d_\theta}$ ;  
**Require:** Number of projections  $L$ , hyperparameter  $\lambda$ , learning rate  $\epsilon$ , number of iterations  $M$ ;

- 1: Initialize  $D=0, L_\lambda=0, m=1$ ;
- 2: **while**  $\omega$  has not converged and  $m \leq M$  **do**
- 3:     Draw a set of samples  $\{\theta_l\}_{l=1}^L$  from  $\mathbb{S}^{d_\theta-1}$ ;
- 4:     **for**  $n=1$  to  $N$  **do**
- 5:         Compute  $g_\omega(x_n)$  and  $g_\omega(y_n)$ ;
- 6:         Calculate the regularization term  $L_\lambda \leftarrow L_\lambda + \frac{\lambda}{N} (\|g_\omega(x_n)\|_2 + \|g_\omega(y_n)\|_2)$ ;
- 7:     **end for**
- 8:     **for**  $l=1$  to  $L$  **do**
- 9:         Compute  $\beta(x_n, \theta_l) = \langle g_\omega(x_n), \theta_l \rangle, \beta(y_n, \theta_l) = \langle g_\omega(y_n), \theta_l \rangle$  for each  $n$ ;
- 10:         Sort  $\beta(x_n, \theta_l)$  and  $\beta(y_n, \theta_l)$  in ascending order s.t.  $\beta(x_{I_x^l[n]}, \theta_l) \leq \beta(x_{I_x^l[n+1]}, \theta_l)$  and  $\beta(y_{I_y^l[n]}, \theta_l) \leq \beta(y_{I_y^l[n+1]}, \theta_l)$ ;
- 11:         Calculate the ASWD:  $D \leftarrow D + (\frac{1}{L} \sum_{n=1}^N |\beta(x_{I_x^l[n]}, \theta_l) - \beta(y_{I_y^l[n]}, \theta_l)|^k)^{\frac{1}{k}}$ ;
- 12:     **end for**
- 13:      $\mathcal{L} \leftarrow D - L_\lambda$ ;
- 14:     Update  $\omega$  by gradient ascent  $\omega \leftarrow \omega + \epsilon \cdot \nabla_\omega \mathcal{L}$ ;
- 15:     Reset  $D=0, L_\lambda=0$ , update  $m \leftarrow m+1$ ;
- 16: **end while**
- 17: Draw a set of samples  $\{\theta_l\}_{l=1}^L$  from  $\mathbb{S}^{d_\theta-1}$ ;
- 18: **for**  $n=1$  to  $N$  **do**
- 19:     Compute  $g_\omega(x_n)$  and  $g_\omega(y_n)$ ;
- 20: **end for**
- 21: **for**  $l=1$  to  $L$  **do**
- 22:     Compute  $\beta(x_n, \theta_l) = \langle g_\omega(x_n), \theta_l \rangle, \beta(y_n, \theta_l) = \langle g_\omega(y_n), \theta_l \rangle$  for each  $n$ ;
- 23:     Sort  $\beta(x_n, \theta_l)$  and  $\beta(y_n, \theta_l)$  in ascending order s.t.  $\beta(x_{I_x^l[n]}, \theta_l) \leq \beta(x_{I_x^l[n+1]}, \theta_l)$  and  $\beta(y_{I_y^l[n]}, \theta_l) \leq \beta(y_{I_y^l[n+1]}, \theta_l)$ ;
- 24:     Calculate the ASWD:  $D \leftarrow D + (\frac{1}{L} \sum_{n=1}^N |\beta(x_{I_x^l[n]}, \theta_l) - \beta(y_{I_y^l[n]}, \theta_l)|^k)^{\frac{1}{k}}$ ;
- 25: **end for**
- 26: **Output:** Augmented sliced Wasserstein distance  $D$ .

---

## Appendix D Experimental setups

### D.1 Hyperparameters in the sliced Wasserstein flow experiment

We randomly generate 500 samples both for target distributions and source distributions. We initialize the source distributions  $\mu_0$  as standard normal distributions  $\mathcal{N}(0, I)$ , where  $I$  is a 2-dimensional identity matrix. We update source distributions using Adam optimizer [Kingma and Ba, 2015], and set the learning rate=0.002. For all methods, we set the order  $k = 2$ . When testing the ASWD, the number of iterations  $M$  in Algorithm 1 is set to 10. Empirical errors in the experiment are found to be not sensitive to the choice of  $\lambda$  in a candidate set of {0.01, 0.05, 0.1, 0.5}. The reported results are produced with  $\lambda = 0.1$ .

### D.2 Network architecture in the generative modeling experiment

Denote a convolutional layer whose kernel size is  $s$  with  $C$  kernels by  $Conv_C(s \times s)$ , and a fully-connected layer whose input and output layer have  $s_1$  and  $s_2$  neurons by  $FC(s_1 \times s_2)$ . The network structure used in the generative modeling experiment is configured to be the same as described in [Nguyen et al., 2020]:

$$\begin{aligned}
h_\psi : (64 \times 64 \times 3) &\rightarrow Conv_{64}(4 \times 4) \rightarrow LeakyReLU(0.2) \rightarrow Conv_{128}(4 \times 4) \rightarrow BatchNormalization \\
&\rightarrow LeakyReLU(0.2) \rightarrow Conv_{256}(4 \times 4) \rightarrow BatchNormalization \rightarrow LeakyReLU(0.2) \rightarrow \\
&Conv_{512}(4 \times 4) \rightarrow BatchNormalization \rightarrow Tanh \xrightarrow{Output} (512 \times 4 \times 4) \\
D_\Psi : Conv_1(4 \times 4) &\rightarrow Sigmoid \xrightarrow{Output} (1 \times 1 \times 1) \\
G_\Phi : z \in \mathbb{R}^{32} &\rightarrow ConvTranspose_{512}(4 \times 4) \rightarrow BatchNormalization \rightarrow ReLU \rightarrow \\
&ConvTranspose_{256}(4 \times 4) \rightarrow BatchNormalization \rightarrow ReLU \rightarrow ConvTranspose_{128}(4 \times 4) \rightarrow \\
&BatchNormalization \rightarrow ReLU \rightarrow ConvTranspose_{64}(4 \times 4) \rightarrow BatchNormalization \rightarrow \\
&ConvTranspose_3(4 \times 4) \rightarrow Tanh \xrightarrow{Output} (64 \times 64 \times 3) \\
\phi : FC(8192 \times 8192) &\xrightarrow{Output} (8192)-dimensional vector
\end{aligned}$$

We train the models with the Adam optimizer [Kingma and Ba, 2015], and set the batch size to 512. Following the setup in [Nguyen et al., 2020], the learning rate is set to 0.0005 and beta=(0.5, 0.999) for both CIFAR10 dataset and CELEBA dataset. For all methods, we set the order  $k$  to 2. For the ASWD, the number of iterations  $M$  in Algorithm 1 is set to 5. The hyperparameter  $\lambda$  is set to 0.5 to introduce slightly larger regularization of the optimization objective due to the small output values from the feature layer  $h_\psi$ .

## Appendix E Additional results in the sliced Wasserstein flow experiment

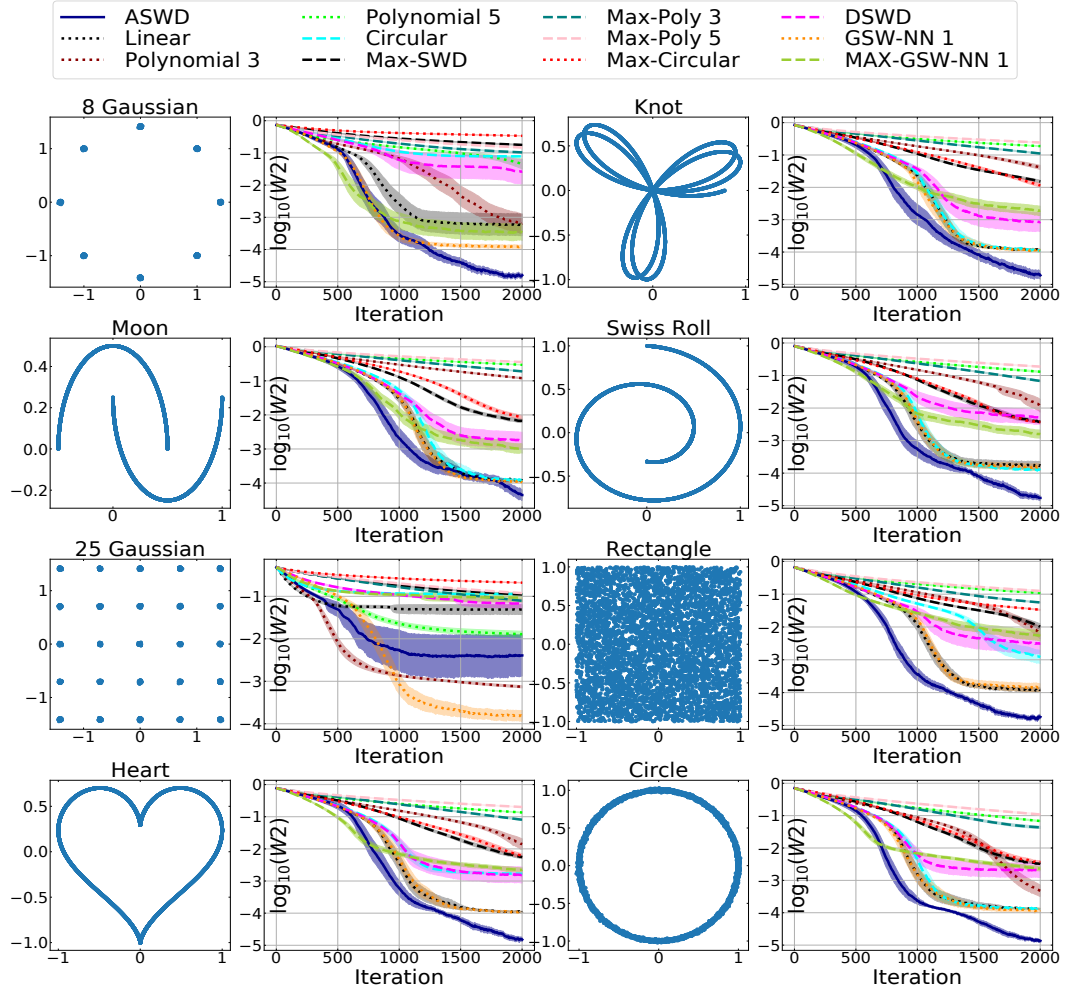


Figure 4: Full experimental results on the sliced Wasserstein flow example. The first and third columns are target distributions. The second and fourth columns are log 2-Wasserstein distances between the target distributions and the source distributions. The horizontal axis shows the number of training iterations. Solid lines and shaded areas represent the average values and 95% confidence intervals of log 2-Wasserstein distances over 50 runs.

## Appendix F Additional results in the generative modeling experiment

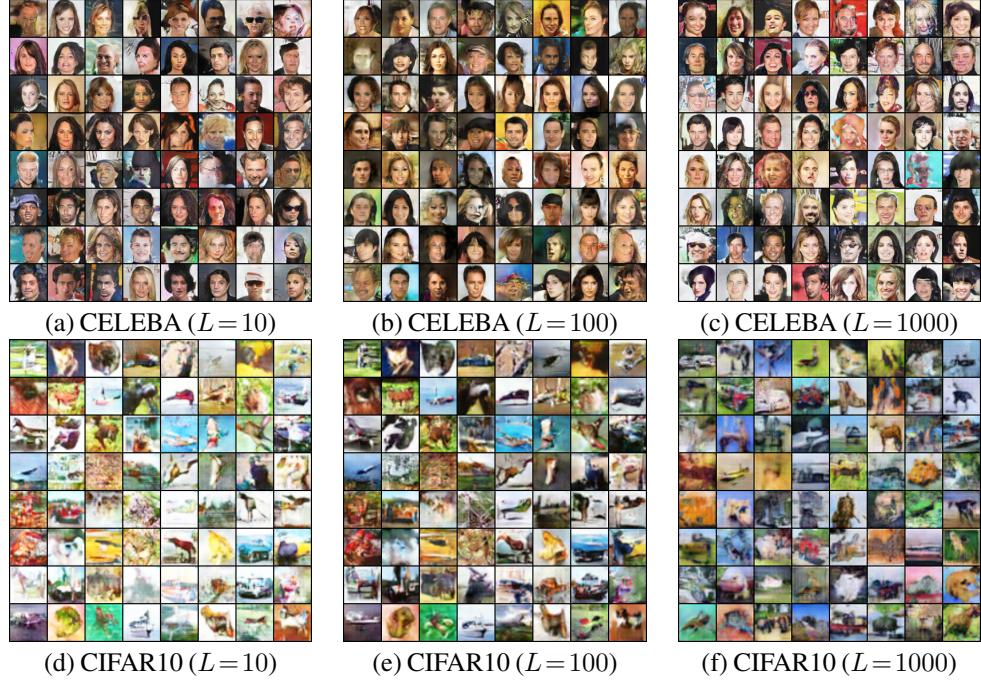


Figure 5: Visualized experimental results of the ASWD on CELEBA and CIFAR10 dataset with 10, 100, 1000 projections. The first row shows randomly selected samples of generated CELEBA images, the second row shows randomly selected samples of generated CIFAR10 images.